




Supplementary Information: Dynamic assembly of nanoparticles with a high-performance Langmuir-Blodgett process: Analysis of the system hydrodynamics with four different optical techniques

O. Lebaigue^{1,*} , O. Delléa^{1,2,*}  and J.M. Delhaye³ 

We have enclosed a series of figures to complement the main paper. When it makes sense, the figure numbering follows the figure numbering of the main paper, *e.g.*, Figures 1bis, 1ter and 1quater are companion figures of Figure 1 of the main paper. As a result, the figure numbering below is not continuous.

List of the additional figures

Fig. 1bis. The trailblazing LB process.

Fig. 1ter. Schematic representation of roll-to-roll LB process with static liquid.

Fig. 1quater. Representation of the roll-to-roll LB process with a flowing subphase.

Fig. 5bis. Schematic of liquid thickness measurement with chromatic confocal microscopy – Case of an HCP particle bed.

Fig. 5ter. Schematic of liquid thickness measurement with chromatic confocal microscopy – Case of a thin film floating on the liquid surface (Parafilm®).

Fig. 7bis: Moiré setup for projection of black and red fringes.

Fig. 12bis: (A) Irregular pattern of particles obtained by producing nanopillars on TiO₂ xerogel by UV insolation through nanospheres (Shavdina, 2016). (B) Grains, grain orientations (blue arrows), and grain boundaries within an HCP film observed with SEM (Désage *et al.*, 2014).

Fig. 13bis: Some pictures of the $m = -1$ order with a white light illumination spot slightly downstream of the hydraulic jump.

Fig. 16bis: Another illustration of the size of the HCP crystalline zones – The sample is 50x50 mm² large, and the typical dimension of the mono-crystals is 500 μm (ranging from 100 μm to more than 5 mm).

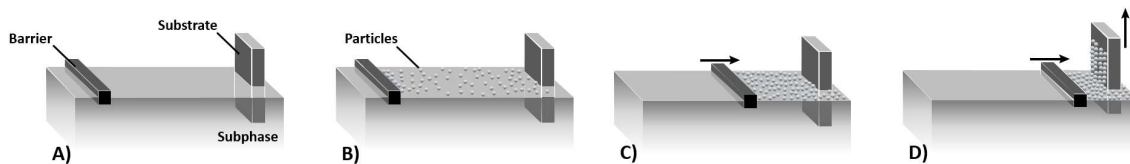


Fig. 1bis. The original LB process: (A) A moving barrier is positioned at the air-subphase interface, and a vertical substrate is partially immersed. (B) Particles are spread over the air-subphase interface. (C) The moving barrier pushes the particles and gradually reduces the space between them. (D) When the nanoparticles form a hexagonal lattice, the substrate is withdrawn at the same speed as the barrier's speed and collects the particle lattice.

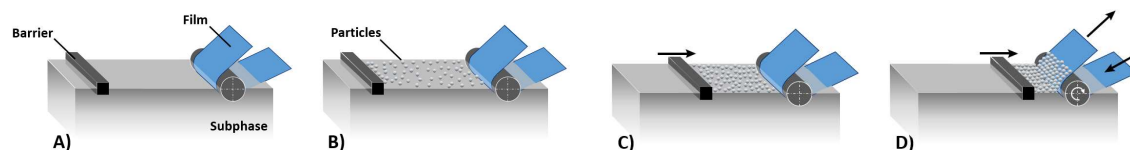


Fig. 1ter. Schematic representation of roll-to-roll LB process with static liquid: (A) A moving barrier is positioned on the air-subphase interface, and a solid film substrate in contact with a roller is partially immersed in the subphase. (B) Particles are spread over the interface. (C) The moving barrier reduces the inter-particle space to obtain an HCP monolayer. (D) The rotating roller transfers the monolayer onto the film while the barrier moves to maintain a constant push. In the above sketches, the other rolls used to put the conveyor film in tension are not represented.

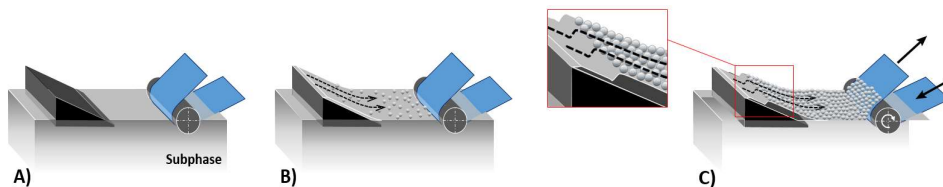


Fig. 1quater. Representation of the roll-to-roll LB process with a flowing subphase: A ramp and a roller-driven film are partially immersed in the subphase. (A) The liquid subphase flows in a laminar regime down the ramp. It receives continuously spread particles on its upper part. (B) The accumulation of particles at the liquid surface and the compression due to the subphase movement lead to a compact monolayer. (C) The rotating roller continuously transfers the monolayer.

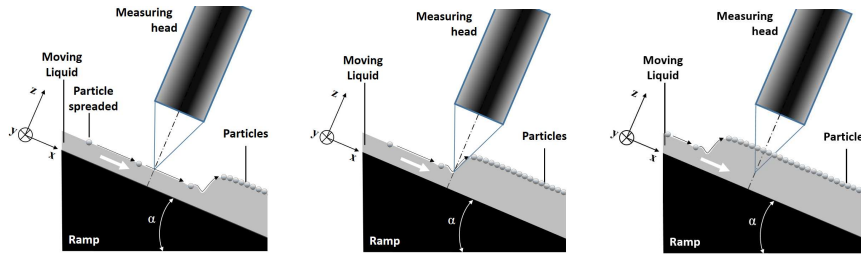


Fig. 5bis. Schematic of liquid thickness measurement with chromatic confocal microscopy – Case of an HCP particle bed. The measuring head is fixed and perpendicular to the ramp. The accumulation of particles on the top of the ramp moves the hydraulic jump from downstream to upstream of the measurement point.

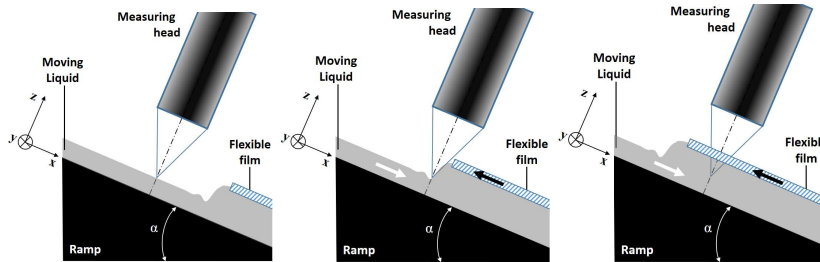


Fig. 5ter. Schematic of liquid thickness measurement with chromatic confocal microscopy – Case of a thin film floating on the liquid surface (Parafilm®). The measuring head is fixed and perpendicular to the ramp. The flexible film moves the hydraulic jump under the measurement point.

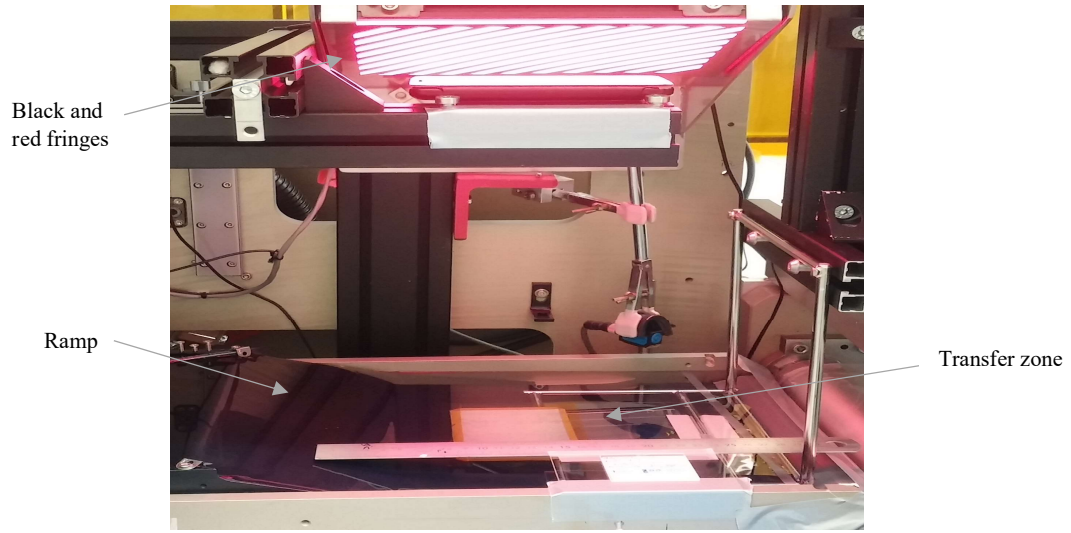


Fig. 7bis: Moiré setup for projection of black and red fringes.

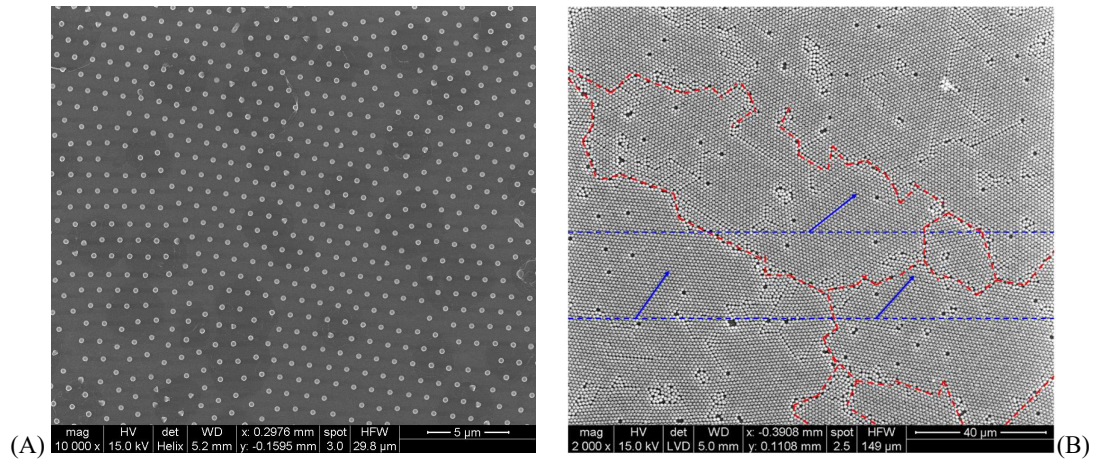


Fig. 12bis: (A) Irregular pattern of particles obtained by producing nanopillars on TiO₂ xerogel by UV insolation through nanospheres (Shavdina, 2016). (B) Grains, grain orientations (blue arrows), and grain boundaries within an HCP film observed with SEM (Désage *et al.*, 2014).

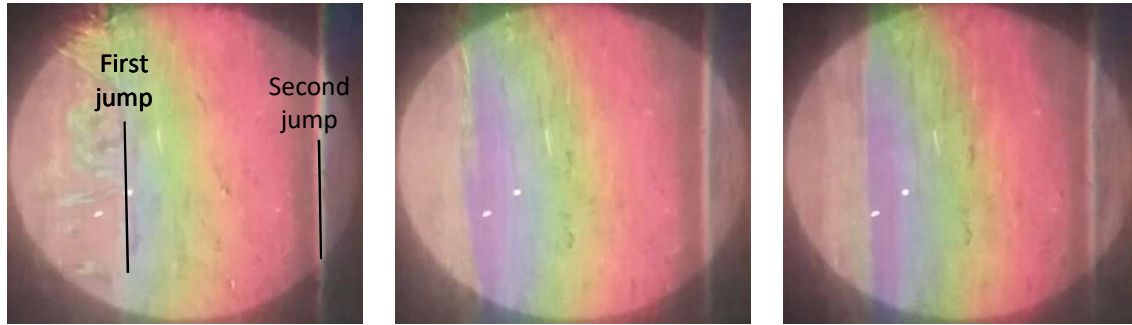


Fig. 13bis. Some pictures of the $m = -1$ order with a white light illumination spot slightly downstream of the hydraulic jump. From left to right: Re *ca.* 17, 28 and 40. The first hydraulic jump is approximately at $1/4$ right from the left border of the pictures.

For values of the Reynolds number Re used in this figure (*ca.* 17, 28 and 40), the non-dimensional shear stress T_p are approximately 0.54, 0.64 and 0.71. There is no substantial increase in the shear stress, especially compared to the capillary forces between the particles, and a more delicate experimental approach is needed to exhibit the effect of the shear stress, as shown in the main paper. However, it has been verified experimentally that the lowest values of the Reynolds number within the range of possible values ($Re = 6, 12$ and 17) are less efficient in assembling the particle. In contrast, Re values of 28, 34 or 40 are more potent. The higher Re values of 46 and 52 are usually less used due to the occurrence of a more wavy film flow regime.

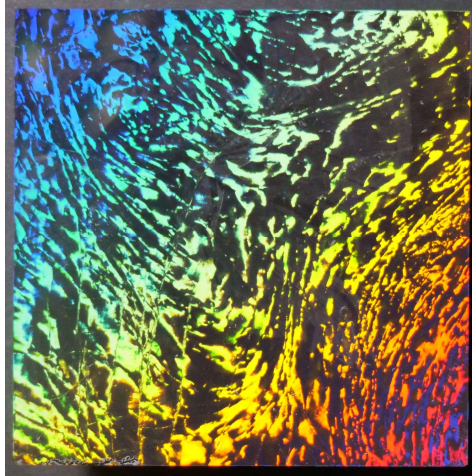


Fig. 16bis: Another illustration of the size of the HCP crystalline zones – The sample is 50x50 mm² large, and the typical dimension of the mono-crystals is 500 μm (ranging from 100 μm to more than 5 mm).